Solution Structure of the Human Oncogenic Protein Gankyrin Containing Seven Ankyrin Repeats and Analysis of Its Structure−Function Relationship[†,‡]

Chunhua Yuan,[*,§,||,⊥] Junan Li,[⊥,#,◆] Anjali Mahajan,[@] Ming Jye Poi,[+] In-Ja L. Byeon,[||,●] and Ming-Daw Tsai[*,§,||,#,@,+,○]

Department of Chemistry, Department of Biochemistry, Biophysics Program, Ohio State Biochemistry Program, and Campus Chemical Instrument Center, The Ohio State University, Columbus, Ohio 43210, and Genomics Research Center, Academia Sinica, Taipei, Taiwan

Received April 30, 2004; Revised Manuscript Received July 8, 2004

ABSTRACT: Human gankyrin (226 residues, 24.4 kDa) is a liver oncoprotein that plays an important role in the development of human hepatocellular carcinomas. In this paper, its solution structure is reported, which is the largest ankyrin protein ever determined by NMR. The highly degenerate primary sequences of the seven ankyrin repeats presented a major challenge, which was overcome by combined use of TROSY experiments, perdeuterated samples, isotope-filtered NMR experiments, and residual dipolar couplings. The final structure was of high quality, with atomic rmsds for the backbone (N, C′, and C^{α}) and all heavy atoms (residues 4−224) of 0.69 ± 0.09 and 1.04 ± 0.09 Å, respectively. Detailed analyses of NMR data suggested that the conserved TPLH motifs play important structural roles in stabilizing the repeating ankyrin scaffold. Gankyrin is conformationally more stable than the tumor suppressor $p16^{INK4A}$, possibly due to the structural roles of conserved residues evidenced by slowly exchanging backbone amides as well as hydrogen bonding networks involving labile side chain protons. Structural comparison with $p16^{INK4A}$ identified several residues of gankyrin that are potentially important for CDK4 binding, whereas observation of the thiol proton of C180 indicated a well-structured Rb-binding site in the helical region of the sixth ankyrin repeat. Interestingly, the CDK4-binding site and Rb-binding site located in N- and C-terminal regions, respectively, are separated by comparatively more stable ankyrin repeats and highly condensed positive surface charge. These results and analyses will shed light on the structural basis of the function of human gankyrin.

Human gankyrin is a liver oncoprotein that plays an important role in the development of hepatocellular carcinomas (*1*). Overexpression of gankyrin has been observed in all studied human and rodent hepatocellular carcinomas, and has been further correlated with increases in the levels of both phosphorylation and degradation of tumor suppressor retinoblastoma protein (Rb) (*1*−*3*). In relation to these effects, gankyrin has been shown to interact with three components in the Rb pathway, namely, Rb, the S6 ATPase subunit of the 26S proteasome, and cyclin-dependent kinase 4 (CDK4)[1] (*1*, *4*, *5*). From *in vitro* studies, dual functional roles have been proposed for gankyrin in the expanded INK4-CDK4/6-Rb pathway (*5*). On one hand, gankyrin binds to both tumor suppressor Rb and the S6 ATPase subunit of the 26S proteasome, which in turn facilitates CDK4/6-mediated Rb phosphorylation and drives Rb into ubiquitin-mediated degradation. On the other hand, gankyrin directly interacts with CDK4 and counteracts the inhibitory function of $p16^{INK4A}$ and $p18^{INK4C}$. Moreover, it has been shown that the oncogenic activity of gankyrin can be suppressed by binding to melanoma antigen (MAGE)-A4, a tumor specific antigen with potential in antitumor immunotherapy (*6*). These findings taken together strongly suggest that gankyrin is a promising target for developing novel therapeutic strategies against liver cancers.

[†] This work was supported by NIH Grant CA69472 (to M.-D.T.). The Bruker DRX-800 NMR spectrometer was funded by Ohio Board of Regents, and the Bruker DMX-600 spectrometer was funded by NIH Grant RR08299. Structural calculation performed in the Ohio Supercomputer Center was supported by the BALE Cluster supercomputer resource grant.

[‡] PDB entry 1TR4. Backbone chemical shift assignments (^{15}N, $^{1}H^{N}$, $^{13}C'$, $^{13}C^{\alpha}$, $^{13}C^{\beta}$, and $^{1}H^{\alpha}$) accession code BMRB-5898.

* To whom correspondence should be addressed: Department of Chemistry, The Ohio State University, 100 West 18th Ave., Columbus, OH 43210. E-mail: cyuan@ccic.ohio-state.edu and tsai.7@osu.edu.

[§] Department of Chemistry, The Ohio State University.

[||] Campus Chemical Instrument Center, The Ohio State University.

[⊥] These authors contributed equally to this work.

[#] Department of Biochemistry, The Ohio State University.

[◆] Current address: Department of Surgery, College of Medicine, The Ohio State University, Columbus, OH 43210.

[@] Biophysics Program, The Ohio State University.

[+] Ohio State Biochemistry Program, The Ohio State University.

[●] Current address: Building 5, Room B2-41, National Institutes of Health, Bethesda, MD 20892.

[○] Academia Sinica.

[1] Abbreviations: 2D, two-dimensional; 3D, three-dimensional; AR, ankyrin repeat; CDK4/6, cyclin-dependent kinase 4/6; CSI, chemical shift index; GST, glutathione *S*-transferase; HMBC, heteronuclear multiple-bond correlation; HSQC, heteronuclear single-quantum coherence spectroscopy; INK4, inhibitor of cyclin-dependent kinase 4; NMR, nuclear magnetic resonance; NOE, nuclear Overhauser effect; NOESY, NOE spectroscopy; Rb, retinoblastoma protein; RDC, residual dipolar coupling; rmsd, root-mean-square deviation; TOCSY, total correlation spectroscopy; TROSY, transverse relaxation-optimized spectroscopy.

10.1021/bi049116o CCC: $27.50
Published on Web 08/28/2004

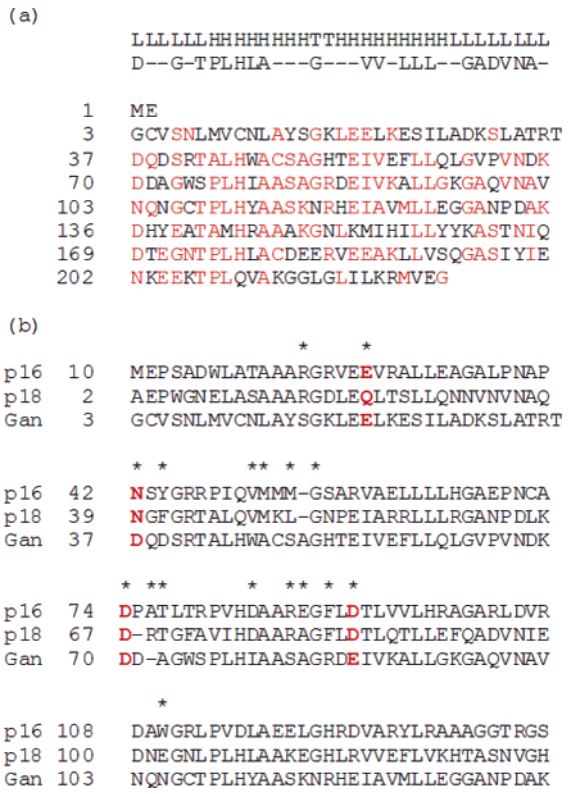

FIGURE 1: (a) Primary sequence of gankyrin with repeating residues in AR highlighted in red. The AR consensus sequence and the typical secondary conformation (H, T, and L representing helix, turn, and loop, respectively) are shown at the top (*7*). (b) Structure-based sequence alignment of $p16^{INK4A}$, $p18^{INK4C}$, and gankyrin in the CDK4-binding site. The asterisks denote the residues of $p16^{INK4A}$ identified at the $p16^{INK4A}$−CDK6 complex interaction interface (*43*). The alignment identifies four residues (in red) in gankyrin that likely use their side chains in forming hydrogen bonds with CDK4.

From analysis of the primary sequence (Figure 1a), six ankyrin repeats (AR) can be identified, each containing a characteristic TPLH tetrapeptide or a variance (*1*, *7*). The ankyrin repeat is a 33-residue repeating motif, defined as a β-hairpin−helix−turn−helix structure (*7*). The helix−turn−helix seems to be the core of the repeat, in which the two α-helices are antiparallel and stacked side by side. First reported in 1987, the ankyrin repeat has been identified as one of the most abundant structure motifs in proteins from eukaryotes that have very diverse functions, e.g., CDK4/6 inhibitor $p16^{INK4A}$ and transcriptional regulator GABP-β (*7*, *8*). Ankyrin proteins typically consist of four to six repeats linearly stacked together and usually play a key role in mediating protein−protein interactions. Gankyrin, in contrast to INK4 and other ankyrin proteins that have only one functional domain, binds to multiple partners to promote cell cycle control as briefed above. To understand its functional role and its intricate relationship with other ankyrin proteins for CDK4 binding (e.g., $p16^{INK4A}$ and IκBα) from structural perspectives (*5*, *9*), it is important to determine the tertiary structure of gankyrin under physiological conditions.

We here report the tertiary structure of gankyrin determined by multidimensional NMR spectroscopy, which reveals seven ankyrin repeats (numbered AR1−AR7 starting from N-terminus) with some structural variance in the capping units. The results are significant. (i) Hydrogen bonds involving the side chains of Thr and His residues in a TPLH motif were deduced from resonance and NOE assignments, underscoring the role of highly conserved residues in the structural integrity of an ankyrin repeat. (ii) Stabilizing features such as amino−aromatic interactions were uncovered in the capping units, which could be significant for ankyrin repeat protein design. (iii) Structural comparison with $p16^{INK4A}$ has identified several putative residues in AR1−AR3 of gankyrin that are potentially important for CDK4 binding. (iv) The Rb-binding motif LXCXE was identified in the first helix of AR6, and C180 was found in a reduced form with its thiol proton observed. (v) Finally, between the CDK4- and Rb-binding sites, a more stable loop conformation as well as more condensed positive surface charge was observed in AR4 and AR5.

MATERIALS AND METHODS

Sample Preparation. Full-length human gankyrin (residues 1−226) was expressed as a glutathione *S*-transferase (GST) fusion protein, and the GST tag was removed, leaving GPLGS residues at the N-terminus of gankyrin (*5*). [U-^{15}N]-, [U-^{13}C,^{15}N]-, and [U-^{13}C,^{15}N,70% ^{2}H]-labeled gankyrin were expressed and purified essentially as described previously (*5*) except that the bacteria harboring the expression vector were grown at 37 °C in M9 minimal medium containing 1.0 g/L [^{15}N]ammonium sulfate with or without 1.5 g/L [$^{13}C_6$]glucose and 80% (v/v) $^{2}H_2O$. The protein concentrations were 0.3−0.6 mM in 5 mM HEPES, 1 μM EDTA, and 1 mM DTT (pH 7.4). A higher concentration results in visible aggregation.

NMR Spectroscopy. The lyophilized gankyrin samples were dissolved in either 90% H_2O and 10% $^{2}H_2O$ or 100% $^{2}H_2O$. The NMR spectra were collected at 300 K on a Bruker DMX-600 spectrometer as well as on a Bruker DRX-800 spectrometer, each of which is equipped with a 5 mm triple-resonance probe with three-axis gradients. The TROSY-based triple-resonance experiments, including TROSY-HNCA, TROSY-HN(CO)CA, TROSY-HNCO, TRSOY-HNCACB, and TROSY-HN(CO)CACB, were carried out with the [U-^{13}C,^{15}N,70% ^{2}H]-labeled sample for sequential assignment (*10*). 3D ^{15}N-edited TOCSY and 3D HCCH-TOCSY were carried on [U-^{15}N]- and [U-^{13}C,^{15}N]-labeled samples, respectively, for side chain chemical shift assignment. 3D ^{15}N-edited NOESY data sets were collected on a [U-^{15}N]-labeled sample with two mixing times of 100 and 200 ms, and on a [U-^{13}C,^{15}N,70% ^{2}H]-labeled gankyrin with a mixing time of 150 ms. 3D ^{13}C-edited NOESY data sets were recorded with a [U-^{13}C,^{15}N]-labeled sample dissolved in 90% H_2O and 10% $^{2}H_2O$ as well as in 100% $^{2}H_2O$, each of which has a mixing time of 100 ms. 2D NOESY spectra were collected in 100% $^{2}H_2O$ or in 90% H_2O and 10% $^{2}H_2O$. Slow ^{1}H−^{2}H exchanging backbone amides were identified by recording ^{1}H−^{15}N HSQC spectra after dissolving the lyophilized protein into 100% $^{2}H_2O$ buffer for a period of time. NMR data were processed with XWINNMR version 3.1 (Bruker, Inc.).

Residual Dipolar Coupling Experiment. Backbone amide residual dipolar coupling (RDC) experiments were performed on the Bruker DRX-800 spectrometer on a [U-^{15}N]-labeled sample in the presence of filamentous Pf1 phage (ASLA Ltd., Riga, Latvia) (*11*). The concentration of phage was ca. 3.5 mg/mL, resulting in a 5 Hz splitting of the $^{2}H_2O$ signal that ensured a weak alignment (*11*, *12*). Doublet-separated sensitivity-enhanced HSQC spectra were collected for the

determination of scalar and dipolar one-bond *J* coupling (*13*). The data were processed with NMRPipe (*14*) and analyzed with NMRView (*15*). Approximate values of the axial and rhombic components of the molecular alignment tensor were determined by the distribution of NH residual dipolar couplings and a grid search (*16*, *17*). The accordance between experimental RDC data and gankyrin NMR structure was evaluated using the program Module (*18*), and the dipolar *R*-factor that measures the agreement between observed and calculated dipolar couplings was calculated (*19*).

Structure Calculation. The solution structures were determined on the basis of distance restraints derived from the identified NOEs and H-bonds, the backbone torsion angle restraints derived from chemical shifts using TALOS (*20*), and residual dipolar coupling constants (*12*, *16*). NOE-derived distance constraints were classified as 1.8−2.7, 1.8−3.7, 1.8−5.0, and 1.8−6.0 Å according to the relative NOE cross-peak intensities. Upper limits for distances involving methyl protons and non-stereospecifically assigned protons were corrected appropriately as described previously (*21*). The structures were calculated utilizing a dynamical annealing protocol (*22*) implemented in CNS (*23*) and analyzed with PROCHECK (*24*) and MOLMOL (*25*). The structure figures were produced using MOLMOL (*25*), and the NMR spectra were generated with XWINNMR (Bruker, Inc.).

RESULTS AND DISCUSSION

A High Level of Intramolecular Sequence Homology Presents a Challenge for NMR Assignments. To date, structures of only five ankyrin repeat proteins, four INK4 members (*26*−*29*) and myotrophin (*30*), have been determined by NMR. Human gankyrin is not only larger in size (24.4 kDa and seven ankyrin repeats) but also higher in its level of internal sequence homology. With the exclusion of the N- and C-capping repeats that typically are less similar to the consensus sequence, the five internal ankyrin repeats are 33.1% identical and 61.8% homologous in terms of the pairwise sequence (Figure 1a). This highly degenerate sequence as well as the modular architecture leads to extensive spectral overlap. The predominant helical rather than β-strand conformation further inhibits chemical shift dispersion and renders resonance assignments difficult.

To overcome these problems, TROSY-based triple-resonance experiments (*10*) on a [U-^{13}C,^{15}N,70% ^{2}H]-labeled sample, which can provide superior spectral resolution and improved effective sensitivity for large proteins, were performed and the data used for sequential assignments. A 3D ^{15}N-edited NOESY experiment conducted on the same perdeuterated sample further improved H^N-H^N NOE walk, due to reduction of ^{15}N relaxation by ^{2}H labeling (*31*). As a result, all but two backbone amides (G150 and G215) have been assigned. For side chain chemical shift assignments, 3D ^{15}N-edited TOCSY and 3D HCCH-TOCSY experiments were conducted and the results analyzed. The 3D C(CO)-NH-TOCSY and H(CCO)NH-TOCSY experiments, however, gave poor results likely due to inefficient coherence transfer. Approximately 65% of the residues have been assigned completely for their side chain resonances, and another 32% have been partially assigned. Spectral degeneracy caused by the high content of helical structure and sequence homology is clearly shown in the ^{1}H−^{15}N HSQC spectrum, where many peaks are overlapping within 0.01 ppm of ^{1}H and 0.1 ppm of ^{15}N chemical shifts, e.g., K23 and N173, I55 and L62, G63 and G96, V89 and I121, Q104 and K203, K116 and A148, and L159 and E225.

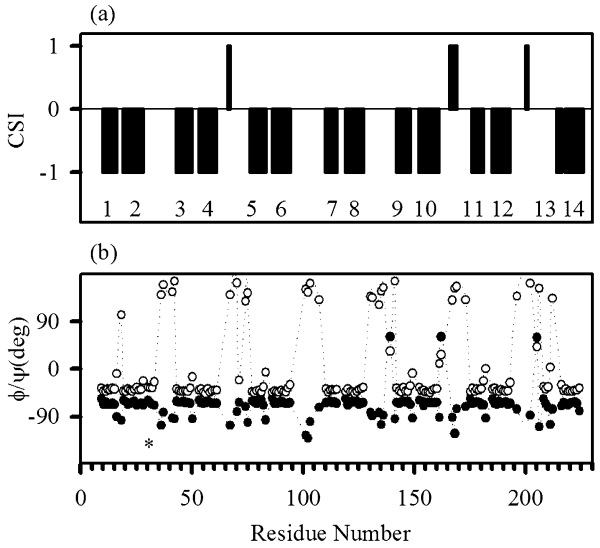

FIGURE 2: Prediction of secondary structures by both the CSI method and TALOS software using backbone chemical shift assignments. (a) Secondary structural elements (+1, −1, and 0 for α-helix, β-strand, and random coil, respectively) from consensus CSI data (*32*). The α-helices identified with the CSI are numbered sequentially. (b) Backbone dihedral angles ϕ (●) and ψ (○) from the TALOS prediction (*20*). The asterisk denotes the four-residue stretch (K30−A33) that appears to adopt a short helical conformation following α-helix 2, which in turn makes the β-hairpin loop one residue longer than that observed in a consensus AR.

The chemical shift index (CSI) method (*32*) and TALOS (*20*) enabled us to derive secondary structures from backbone chemical shift data that are found to be exquisitely sensitive to local conformation (Figure 2). The CSI method, which is based on chemical shift deviations of $^{13}C^{\alpha}$, $^{13}C^{\beta}$, $^{13}C'$, and $^{1}H^{\alpha}$ resonances from respective random coil values, predicted 13 long α-helices (7−10 residues), one short α-helix (~4 residues), and three intercalated short β-strands. Similar results were obtained with TALOS, which predicts backbone dihedral angle values by searching a database for chemical shift ($^{13}C^{\alpha}$, $^{13}C^{\beta}$, $^{13}C'$, $^{1}H^{\alpha}$, and ^{15}N) and sequence homology. The helices derived from chemical shift data were generally supported by short-range NOE assignments such as $H^{\alpha}(i)-H^{N}(i+3)$ and $H^{\alpha}(i)-H^{\beta}(i+3)$, although not all of the expected NOE correlations can be assigned, largely due to overlap of cross-peaks. Nevertheless, the following α-helices were identified with NOE assignments: V10−S16, L19−L28, A42−S49, T53−Q61, P76−S82, D86−G94, P109−S115, H119−E126, A142−A148, L152−Y160, P175−D181, V185−S193, L209−A212, and G217−M223. These in turn form seven helix−turn−helix motifs (the core of seven ankyrin repeats).

Investigation of Histidine and Threonine Residues in the TPLH Tetrapeptide. A salient feature of an ankyrin repeat is the highly conserved TPLH motif. Crystal structures of other ankyrin proteins showed that this motif makes a tight turn to initiate a helix−turn−helix motif, and Thr coupled with His serves as the α-helix N-cap (*7*). However, this motif happens to be absent in the INK4 proteins and myotrophin, the AR proteins whose structures have been determined by

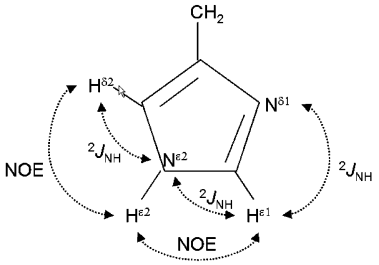

FIGURE 3: Schematic diagram showing the side chain of an $N^{\epsilon 2}$-protonated histidine residue with the dotted arrows indicating NOEs and two-bond $^2J_{HN}$ coupling cross-peaks observed in Figure 4.

NMR. The NMR study presented here provides additional insight into this motif, that the histidine assumes an $N^{\epsilon 2}-H$ tautomeric form (Figure 3) and the threonine receives structural protection for its labile hydroxyl proton.

Figure 4a shows the ^{15}N downfield region of a $^1H-^{15}N$ heteronuclear multiple-bond correlation (HMBC) spectrum optimized for observation of two-bond correlation. Five histidine residues displayed a pattern of the $N^{\epsilon 2}-H$ form, which is characterized by a set of two-bond coupling peaks of $H^{\epsilon 1}-N^{\delta 1}$, $H^{\epsilon 1}-N^{\epsilon 2}$, and $H^{\delta 2}-N^{\epsilon 2}$ (*33*). The corresponding $H^{\epsilon 2}$ protons were observed in the proton downfield region (11−12 ppm) with strong NOEs to both neighboring $H^{\epsilon 1}$ and $H^{\delta 2}$ protons (Figure 4b). Further NOE assignments led to their identification all in a TPLH motif or a variation (Table 1). One of those NOEs was assigned to the interaction between His $H^{\epsilon 2}$ and the Thr H^{α} in the following TPLH motif, which supports the formation of a hydrogen bond between His $H^{\epsilon 2}$ and a distant carbonyl oxygen at the His+29 position, the residue just preceding the TPLH peptide in the next β-hairpin loop (e.g., H177 $H^{\epsilon 2}-$K206 O in Figure 5).

Histidine is also engaged in interactions with threonine in a TPLH motif. An example shown in Figure 5 indicates two reciprocal side chain−backbone hydrogen bonds (Thr H^N-His $N^{\delta 1}$ and Thr $O^{\gamma 1}-$His H^N) and another potential side chain−side chain hydrogen bond (Thr $H^{\gamma 1}-$His $N^{\delta 1}$) deduced from NMR assignments and generated structures. The last hydrogen bond, which was not addressed to the best of our knowledge in any crystal structures of ankyrin protein, is credited to the ability of NMR to detect the protection for the labile hydroxyl proton and the associated NOEs such as the one between T174 $H^{\gamma 1}$ and H177 $H^{\epsilon 1}$. It is important to note that these NMR assignments were challenging due to the nature of oxygen-attached protons. In an attempt to resolve ambiguities, several isotope-filtered NMR experiments have been performed, including 2D $^{13}C-$ and ^{15}N-filtered (f1) and f2 unfiltered NOESY on a [U-^{13}C,^{15}N]-labeled sample and a 2D double half-^{15}N-filtered NOESY on a [U-^{15}N]-labeled sample (*34*, *35*). This body of data taken together with other NOESY data sets allowed us to make unambiguous NMR assignments (Table 1). The observation of S75 H^{γ} in ^{75}SPLH^{78} suggests that a serine residue can also adopt a similar hydrogen bonding network with its side chain. However, threonine is clearly preferred because its buried bulky methyl group could further contribute to stability via hydrophobic interactions with the residue at the Thr+26 position, which is Ala in the ankyrin repeat consensus sequence.

It has been well documented that an amino acid at the N-cap has a significant impact on the stability of α-helical structure (*36*, *37*). In nature, a high frequency of Ser at the N-cap coupled with Glu at the Ser+3 position is found which could provide reciprocal side chain−backbone interactions in stabilizing a helical conformation (*37*). In gankyrin with predominant α-helical elements, the three aforementioned potential hydrogen bonds between Thr and His residues together with one more involving backbone atoms only (Thr O and His H^N) (*38*, *39*) should contribute significantly to secondary structure stability. Moreover, the inter-ankyrin repeat hydrogen bond involving His $H^{\epsilon 2}$ and the hydrophobic interactions involving the methyl group of threonine further contribute to the stabilization of the elongated tertiary fold. Therefore, the NMR data presented here could well explain why the TPLH motif, the Thr and His pair in particular, is highly conserved among ankyrin repeats. The data also nicely complement the results from crystal structures of ankyrin proteins, which can only elucidate information about heavy atoms.

Tertiary Structure of Seven Ankyrin Repeats. The NMR constraints were largely collected from 2D and 3D NOESY spectra recorded in either 100% ^2H_2O or 90% H_2O and 10% ^2H_2O. Effort was made to resolve ambiguous NOEs by using every piece of information and an iterative strategy of structure-assisted assignment. Figure 6 shows an example how an NOE between T108 H^N and H111 $H^{\epsilon 1}$ is assigned, which is comparable to the NOE between T174 H^N and H177 $H^{\epsilon 1}$ indicated in Figure 5. Hydrogen bonds and dihedral angle constraints in the identified secondary structure as well as RDC data of backbone amides were also incorporated in structural calculation. The RDC experiment conducted in a slightly anisotropic environment assesses the one-bond internuclear dipolar interactions which can be correlated with the average orientation of the corresponding vectors relative to the magnetic field (*12*, *40*).

In the first stage, a preliminary low-resolution structure was built with ∼1000 unambiguous NOEs mostly attributed to unique resonances. The structure revealed an elongated globular shape that was used to aid in more NOE assignments; in other words, the candidate for an NOE assignment could be significantly narrowed down to the neighboring repeats. More structure-assisted NOEs were assigned, and then the next-generation structure was calculated. When the NOE number reached ∼1400, an ensemble of 10 calculated structures revealed a backbone (residues 20−200) atomic rmsd value of 2.3 Å. As many as 20 rounds of structure calculations have been performed, during which NOE assignments were added and cross-checked. The final ensemble of 20 structures was selected from a total of 80 calculations based on 3185 constraints, and the structural statistics are summarized in Table 2. The structure has revealed seven ankyrin repeats that linearly stack on each other, with a global architecture reminiscent of p16^{INK4A} (Figure 7). Interactions between short β-strands were observed, but the evidence was not sufficient to propose a continuous β-sheet in hairpin loops. While the internal five ankyrin repeats show a high level of structural similarity and superimpose with an average pairwise root-mean-square deviation (rmsd) of 0.88 Å for backbone atoms, several points about the capping repeats are worth mentioning. (1) The N-terminus is well-folded and appears to consist of a distorted β-strand (Figure 7b). The well-ordered nature is evidenced from resonance and NOE assignments such as

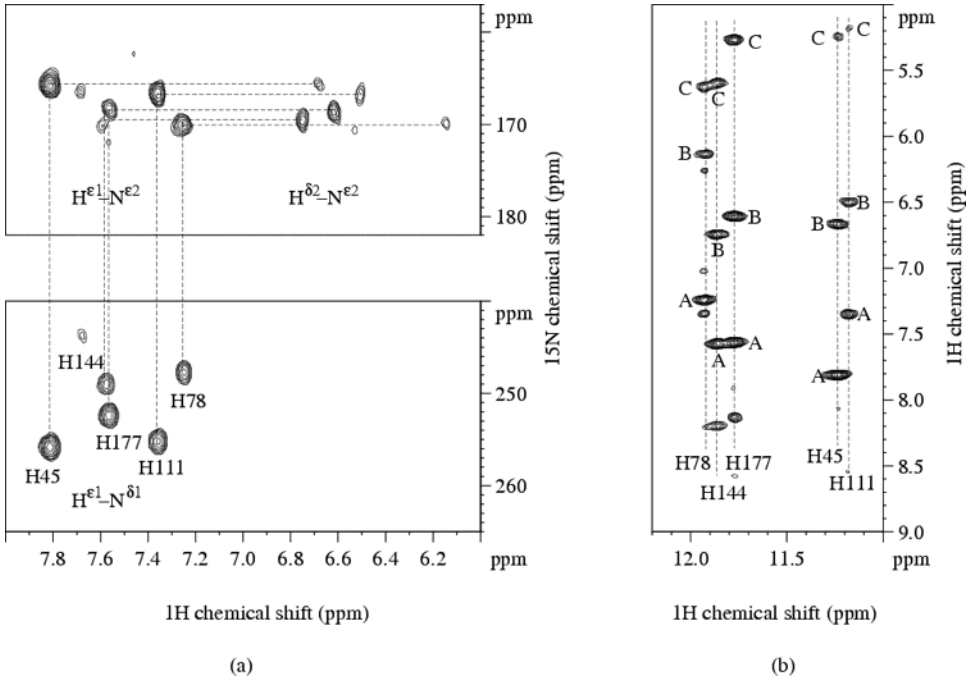

FIGURE 4: Identification of the histidine tautomeric state. (a) $^1H-^{15}N$ HMBC spectrum recorded on a [U-^{15}N]-labeled sample on the Bruker DRX-800 spectrometer with a ^{15}N spectral width of 250 ppm. The $^2J_{HN}$ cross-peak pattern is marked with the dashed line. (b) 2D NOESY spectrum showing the proton downfield region. The cross-peaks designated A−C are NOEs from His $H^{\epsilon 2}$ in a TPLH motif to His $H^{\epsilon 1}$, His $H^{\delta 2}$, and His+30 H^{α} (Thr in the following TPLH motif, e.g., from H177 $H^{\epsilon 2}$ to T207 H^{α}), respectively.

Table 1: Chemical Shift Assignments of Hydroxyl Protons and Imidazole Ring Protons in the TPLH Motif or Its Variants[a]

	Thr $H^{\gamma 1}$ or Ser H^{γ} (ppm)	His $H^{\delta 2}$ (ppm)	His $H^{\epsilon 1}$ (ppm)	His $H^{\epsilon 2}$ (ppm)
^{42}TALH^{45}	6.12	6.68	7.81	11.24
^{75}SPLH^{78}	7.05	6.15	7.27	11.94
^{108}TPLH^{111}	?	6.51	7.36	11.20
^{141}TAMH^{144}	6.40	6.77	7.60	11.86
^{174}TPLH^{177}	6.24	6.62	7.58	11.79
^{207}TPLQ^{210}	5.78	–	–	–

[a] The uncertainty is estimated to be 0.03 ppm for ^1H resonances.

short-range NOEs assigned to E2 and the ring current shift experienced by V5 $H^{\gamma 2}$ (at −0.26 ppm) in the vicinity of Y15 and W46. (2) In the loop following the first helix−turn−helix motif, a four-residue stretch (K30−A33) appears to adopt a helical conformation. As a result, the β-hairpin loop is one residue longer than that observed in a consensus AR. These residues indeed display an average 2.3 ppm upfield shift of $^{13}C^{\alpha}$ resonance from respective random coil values (Figure 2b). However, the NOE data are insufficient for firmly establishing the helical conformation or let alone for differentiating between an α-helix and a 3_{10}-helix. (3) The first α-helix in AR7 is atypically short, leading to a distorted ankyrin repeat. Like the N-terminus, the C-terminal region is also well-folded. Even the backbone amide proton of G226 displays several short-range NOEs.

While it is generally described as "linearly stacking" in ankyrin proteins, a slight bending of the repeat stack toward the β-hairpin loop can be clearly discerned for gankyrin, the largest AR protein structure ever determined by NMR. This observation is impressive considering that as an elongated protein close contacts are made by residues close in primary sequence, and that long-range NOEs can only be observed between adjacent repeats. However, the RDC data in this work have provided an extremely valuablesource of orientation constraints to the overall folding that delineates the slight curvature of the elongated shape (*12*, *16*, *40*). The 2−3° twisting of each ankyrin repeat with respect to the preceding repeat has also been revealed in crystal structures of larger proteins such as human ankyrinR with 12 ankyrin repeats (*41*). When the internal five ankyrin repeats (residues 37−201) of gankyrin are overlaid with human ankyrinR (residues 533−697), the backbone rmsd is only 1.58 Å and the twists along the long molecular axis agree with each other.

Structure−Function Relationship of Gankyrin. Previous *in vitro* studies have narrowed down the CDK4 binding site of gankyrin to the first four ankyrin repeats (gankyrin residues 1−138), and the binding affinity for CDK4 was found to decrease in the following order: $p16^{INK4A}$ > $p18^{INK4C}$ > gankyrin (*5*). Although they share a low degree of homology in sequence, gankyrin and $p16^{INK4A}$ share a high degree of homology in structure. However, aside from different numbers of ankyrin repeats, several major differences are worth noting. (1) $p16^{INK4A}$ has disordered N- and C-termini (*27*, *29*, *42*). (2) The sequence of $p16^{INK4A}$ is less similar to the consensus sequence of an ankyrin repeat, and a repeat unit could be varied by one residue in length. (3) The first helix in the second helix−turn−helix motif of $p16^{INK4A}$ is atypically short. (4) $p16^{INK4A}$ does not have a short helix in the loop following the first helix−turn−helix motif.

On the basis of the $p16^{INK4A}$−CDK6 crystal structure (*43*), the important residues for mediating CDK binding were observed mostly in the first three ankyrin repeats. Those residues using side chains for hydrogen bond formation (R22, E27, N42, D74, D84, R87, and D92 of $p16^{INK4A}$) should contribute significantly to binding specificity as well as binding affinity. It would be instructive to compare gankyrin with $p16^{INK4A}$ to identify prime candidates in gankyrin for

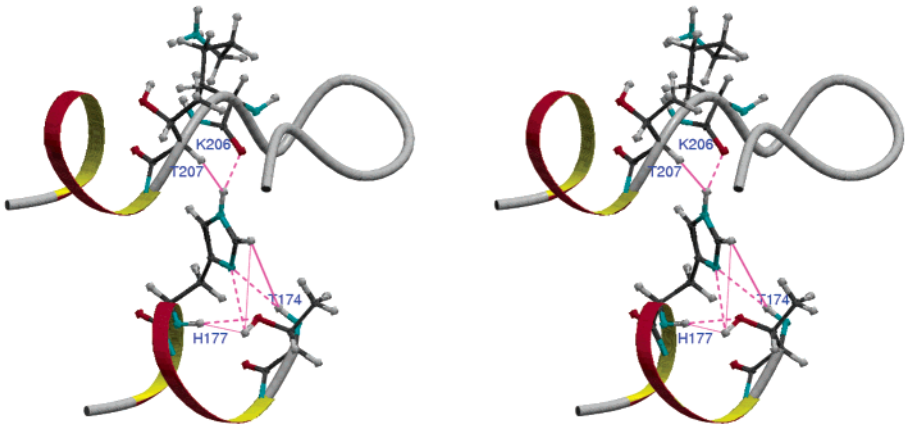

FIGURE 5: Stereoview of a ribbon plot depicting important NOEs as a solid magenta line (T174 H^N−H177 $H^{\epsilon 1}$, T174 $H^{\gamma 1}$−H177 H^N, T174 $H^{\gamma 1}$−H177 $H^{\epsilon 1}$, and H177 $H^{\epsilon 2}$−T207 H^{α}) and potential hydrogen bonds as a dashed magenta line (T174 H^N−H177 $N^{\delta 1}$, T174 $O^{\gamma 1}$−H177 H^N, T174 $H^{\gamma 1}$−H177 $N^{\delta 1}$, and H177 $H^{\epsilon 2}$−K206 O) involving the hydroxyl group and imidazole ring in a TPLH motif. Proton, carbon, nitrogen, and oxygen atoms are colored light gray, dark gray, cyan, and red, respectively. It must be pointed out that the structure shown here was generated without incorporating the constraints of the hydrogen bonds described above.

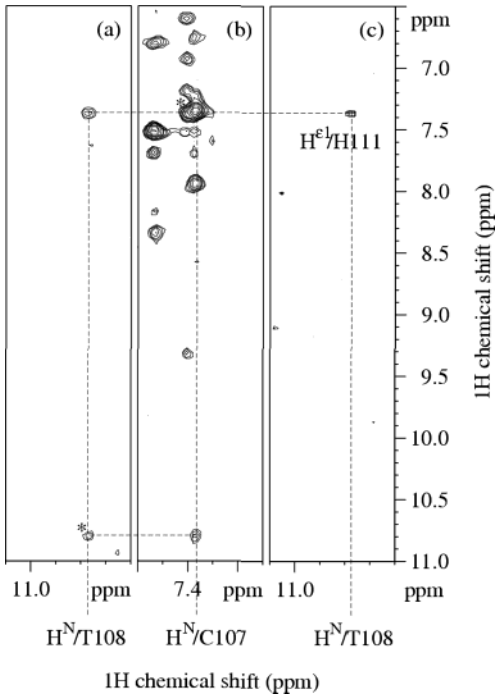

FIGURE 6: Unambiguous NOE assignment between T108 H^N and H111 $H^{\epsilon 1}$ (7.36 ppm) in addition to a H^N−H^N sequential NOE. (a) A slice from a 3D ^{15}N-edited NOESY data set showing the ^{1}H−^{1}H dimensions with ^{15}N at 122.5 ppm. (b) A different slice with ^{15}N at 117.1 ppm. The diagonal peaks of T108 H^N and C107 H^N (7.37 ppm) are marked with asterisks in panels a and b, respectively. (c) ^{15}N-filtered (f1)/^{15}N-selected (f2) data set extracted from a 2D double half-^{15}N-filtered experiment (*34*) performed on a [U-^{15}N]-labeled sample in 90% H_2O and 10% ^2H_2O.

CDK4 binding. Figure 1b shows the structure-based sequence alignment of $p16^{INK4A}$, $p18^{INK4C}$, and gankyrin, while the structural superposition of $p16^{INK4A}$ and gankyrin is shown in Figure 8a. It needs to be pointed out that using AR1−AR3 rather than AR2−AR4 of gankyrin to align with AR1−AR3 of $p16^{INK4A}$ for the CDK4 binding (Figure 1b) leads to a more meaningful alignment and shows that E21, D37, D70, and E87 of gankyrin play roles equivalent to those of E27, N42, D74, and D92, respectively, in $p16^{INK4A}$. Interestingly, E21 and E87 in gankyrin are among the least conserved residues, whereas D37 and D70 are among the highly conserved ones. These putative binding residues will be subjected to further examination by site-directed mutagenesis.

Table 2: Structural Statistics of 20 Gankyrin Structures

restraint	
long-range NOE ($\|i-j\| \geq 5$)	703
short-range NOE ($1 < \|i-j\| < 5$)	756
sequential NOE ($\|i-j\| = 1$)	644
intraresidue NOE	561
hydrogen bond constraints	77 × 2
dihedral angles[a]	227
backbone amide RDC	140
rmsd for distance restraints (Å)	0.029 ± 0.001
R-factor for RDC (%)[b]	4.1 ± 0.2
rmsd from idealized covalent geometry	
bonds (Å)	0.0034 ± 0.0002
angles (deg)	0.50 ± 0.03
impropers (deg)	0.47 ± 0.04
PROCHECK (Ramachandran plot)	
most favored regions (%)	76.9 ± 1.9
additionally allowed region (%)	18.5 ± 1.9
generously allowed region (%)	3.6 ± 0.9
disallowed region (%)	1.0 ± 0.7
rmsd with respect to mean structure	
backbone (residues 4−224)	0.69 ± 0.09
heavy atom (residues 4−224)	1.04 ± 0.09

[a] The dihedral angle constraints include 111 ϕ and 111 ψ torsion angle restraints derived by using TALOS (*20*) and five χ_1 restraints derived from NOE assignments. [b] $R_{dip} = [\langle (D_{obs} - D_{calc})^2 \rangle / (2\langle D_{obs}^2 \rangle)]^{1/2}$, where D_{obs} are D_{calc} are the observed and calculated RDC values, respectively (*19*).

The Rb-binding site of gankyrin is located in the last two ankyrin repeats (*5*) (Figure 8b). More specifically, a peptide fragment of gankyrin (^{176}LHLACDEERV^{185}), in which LXCXE is a Rb-binding motif, was found to be responsible for Rb binding (*5*). Point mutation of L178, C180, or E182 to Ala has been shown to abolish or significantly reduce the Rb binding affinity of gankyrin (*1*, *5*). Two lines of evidence in this NMR work showed that C180 exists in a reduced form and its sulfhydryl group is well protected from solvent exposure (Figure 8b). First, its $^{13}C^{\beta}$ chemical shift (27.4 ppm) is much closer to the random coil value of a reduced cysteine (28.0 ppm) than that of any other possible state (*44*). Second, through the analysis of the aforementioned 2D ^{13}C- and ^{15}N-filtered (f1) and f2 unfiltered NOESY experiment, the thiol proton of C180 was observed at 2.10 ppm with NOEs to C180 H^N and D181 H^N. The observation could be an

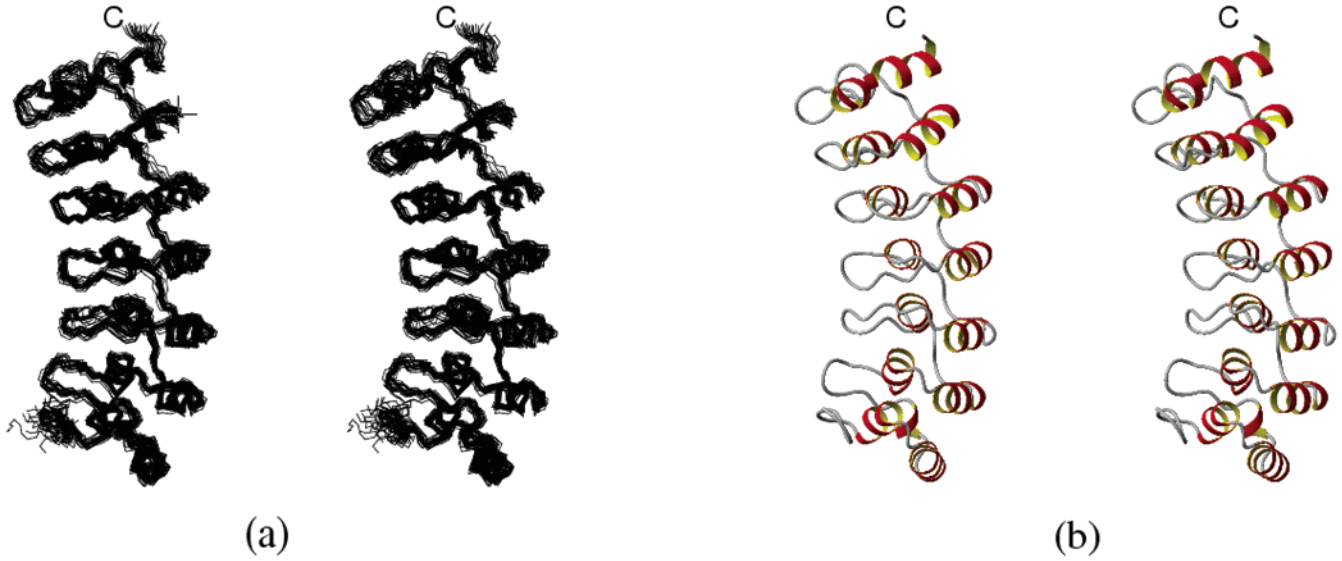

FIGURE 7: (a) Stereoview showing backbone N, C′, and C^{α} atoms of 20 gankyrin structures (residues 1−226). The backbone atoms of residues 4−224 were used for superposition. (b) Stereoview of the ribbon diagram of a representative gankyrin structure.

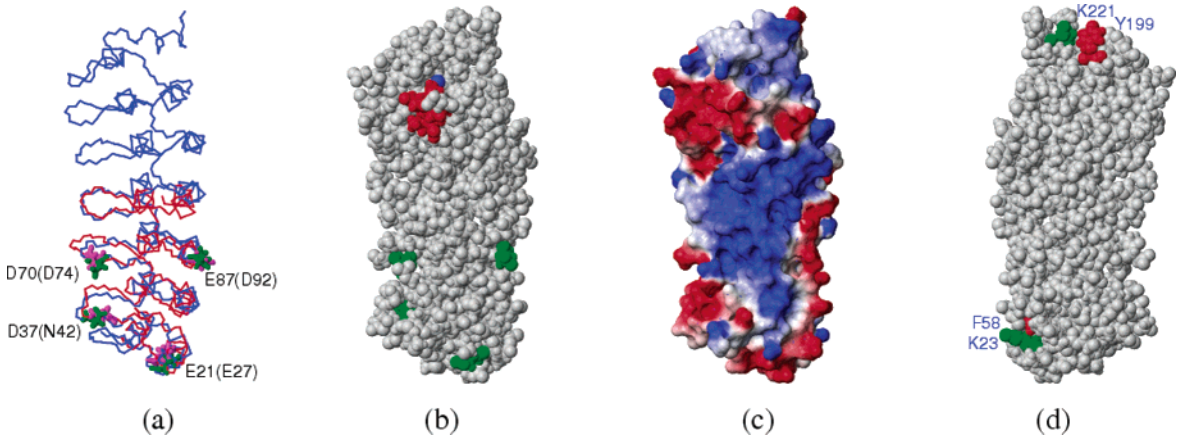

FIGURE 8: (a) Superposition of the backbone atoms of gankyrin (blue, residues 1−226) and $p16^{INK4A}$ (red, residues 14−134) NMR structures (*27*). Residues 8−31, 34−49, 51−70, and 73−106 of gankyrin are superimposed with residues 14−37, 38−54, 55−74, and 78−111 of $p16^{INK4A}$. The backbone rmsd is ca. 2.0 Å for the 94 residues in a span of three ankyrin repeats. The residues potentially important for CDK4 binding are highlighted in green (E21, D37, D70, and E87) and the corresponding residues in $p16^{INK4A}$ in magenta. (b) Rb-binding motif ^{178}LACDE^{182} (highlighted in red) located in the first helix of AR6. C180 S^{γ} is highlighted in blue, and residues E21, D37, D70, and E87 are shown in green. (c) Surface charge distribution. Positive and negative charges are colored blue and red, respectively. (d) Amino−aromatic interactions (K23−F58 and Y199−K221) identified in the capping units. The figures are generated in the same orientation except that panel d is rotated 180° along the long molecular axis.

indication of a well-structured binding site in a helical region and also suggests that in terms of structure the reduced cysteine may be substituted with a structurally equivalent serine residue. Interestingly, the LXSXE motif has been observed in protein phosphatase 1, a Rb-binding protein, and the mutation from LXSXE to LXCXE only increases the binding affinity slightly (*45*). It remains to be established whether the cysteine in the Rb-binding motif can be generally replaced with a serine residue for its functional role.

Stability of Human Gankyrin and Ankyrin Protein Design. In contrast to $p16^{INK4A}$ which displays very low stability and very high conformational flexibility (*46*, *47*), gankyrin is comparatively stable which is evident from the observation of slowly exchanging amide protons. After $^{1}H-^{2}H$ exchange had proceeded at 300 K for 3 h (the lyophilized protein was dissolved in 100% $^{2}H_2O$ buffer), approximately 60 slowly exchanging amide protons could be observed (Figure 9). Most of them are localized in α-helices (Figure 10), and none was found in the vicinity of Gly-induced turn, including two residues N-terminal and four residues C-terminal to the helix-breaking Gly residue. The two projected binding residues, E21 and E87, are both three residues C-terminal to Gly. Interestingly, several residues are clustered in the *β*-hairpin loop interconnecting the fourth and fifth helix−turn−helix motifs: G128, A130, A134, D136, E139, and A140 (Figure 9). They were strongly intense, not just barely observable (Figure 9). It is possible that AR4 and AR5 serve as a "structural scaffold" like the two more stable C-terminal ankyrin repeats, AR3 and AR4, in $p16^{INK4A}$ (*48*). It remains to be established whether this property is related to the fact that AR4 and AR5 of gankyrin divide the CDK4-binding site and the Rb-binding site as we have shown previously (*5*). Coincidently, highly condensed positive charge was also found on the surface of this region, because of several residues in AR4 and AR5 (K116, K118, R145, R149, and K153) (Figure 8c).

Longer $^{1}H-^{2}H$ exchange led to identification of the hydrophobic core in helix−helix packing (Figures 9 and 10).

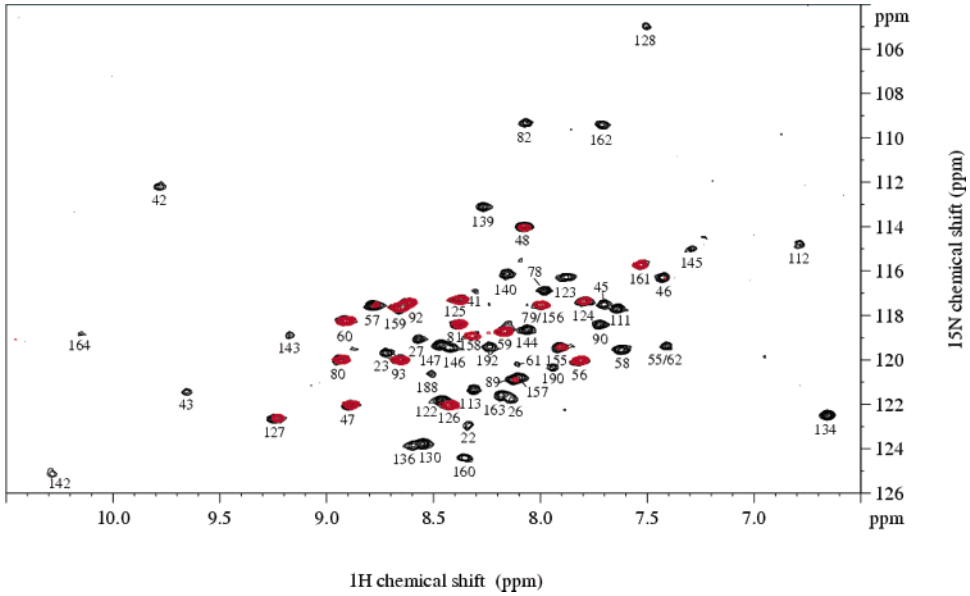

FIGURE 9: Overlay of $^{1}H-^{15}N$ HSQC spectra collected after 3 h (black) and 7 days (red) of $^{1}H-^{2}H$ exchange at 300 K. The backbone amide peaks identified in the latter experiment are A47, C48 (α-helix 3), V56, E57, L59, L60 (α-helix 4), A80, A81 (α-helix 5), V89, L92, L93 (α-helix 6), M124, L125, L126, E127 (α-helix 8), I155, H156, L158, L159 (α-helix 10), and Y161.

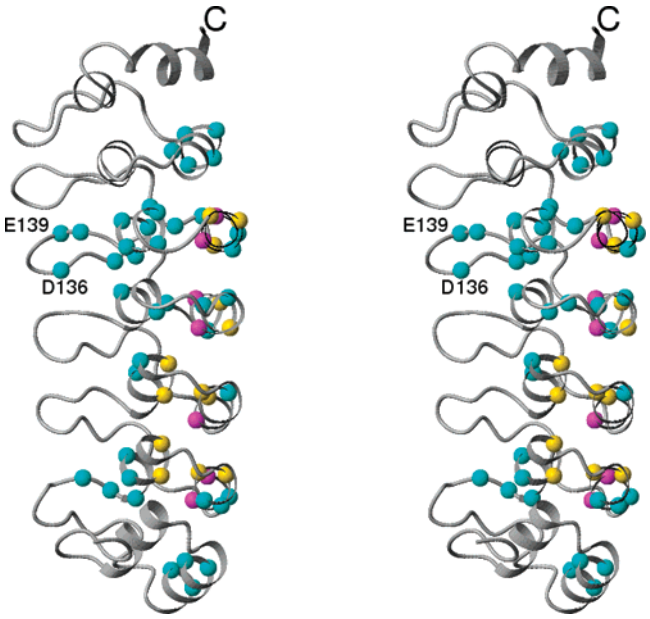

FIGURE 10: Stereoview of the ribbon diagram showing the location of slowly exchanging backbone amides that can be observed after $^{1}H-^{2}H$ exchange for 3 h (cyan), 7 days (gold), and 14 days (magenta) at 300 K.

The backbone amide peaks of L59, L60, L92, L125, L126, L158, and L159 are the only ones that could be detected even after 2 weeks. These Leu residues belong to a homologous pair and are highly conserved in the ankyrin repeats. Together with other conserved residues, particularly the TPLH peptide at the beginning of a helix−turn−helix motif, they could play an important structural role in stabilizing the turn of the L-shaped AR cross section formed by antiparallel α-helices and the extended β-hairpin loop at an approximately right angle.

Though the two capping ankyrin repeats of gankyrin appear to be more flexible from $^{1}H-^{2}H$ exchange data (Figure 10), they are better structured than the two capping repeats of $p16^{INK4A}$. Several features could have been introduced during the evolution to help to stabilize the two termini. (1) Substitution of hydrophobic residues with polar residues in both capping units could avoid the exposure of the hydrophobic surface to solvent. (2) The change from histidine to glutamine in the C-terminal TPLH motif could avoid a destabilizing effect, solvent exposure of the imidazole ring. A similar phenomenon was observed in the last ankyrin repeat of IκBα and other proteins (*49*). (3) Several hydrogen bonds, involving side chains between AR1 and AR2 and between AR6 and AR7, were identified. (4) Two amino−aromatic interactions (*50*) are present between K23 and F58 and between Y199 and K221 in N- and C-termini, respectively (Figure 8d). In favor of this type of interaction, F58 is mostly buried (~4% surface exposure), whereas Y199 has ~42% surface exposure. Furthermore, the exposed amino groups of K23 and K221 could also increase the protein solubility at physiological pH (*51*).

There has been intense interest in designing repeat proteins with novel functionality (*52*). The ankyrin repeat, one of the major modular repeat proteins, has been one of these subjects. Recent work has revealed consensus sequences of building blocks (*38*, *53*), which has significantly advanced our knowledge of ankyrin proteins. Apparently, the design of the capping unit is more challenging since the sequence should be varied to take stability, solubility, and function into consideration (*38*, *39*, *51*, *53*). This could explain why a terminal capping unit is so divergent in the primary sequences of natural proteins. The features uncovered in gankyrin and other ankyrin proteins would be valuable in guiding the design of capping units.

Comparison with X-ray Crystal Structures. During the structural refinement and preparation of the manuscript, two crystal structures of human gankyrin (*54*, *55*) and another crystal structure of a gankyrin homologue (Nas6p) (*56*) were reported. These developments support the significance of gankyrin and provide a good opportunity to compare crystal and solution structures from independent research. As shown in Figure 11, the overall folds of gankyrin structures determined by NMR and X-ray crystallography appear to be very similar with an rmsd value of 1.58 Å for backbone

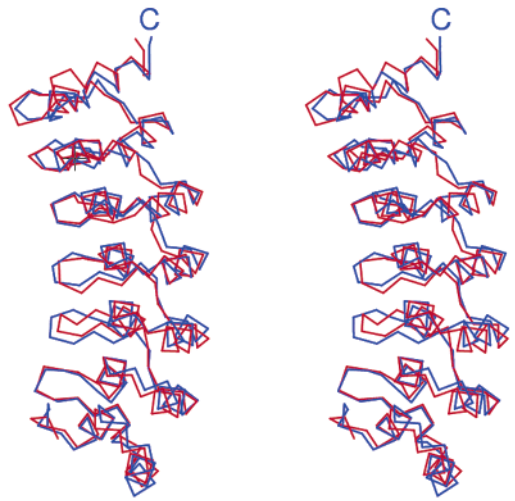

FIGURE 11: Stereoview showing the superposition of the C^{α} trace (residues 4−226) of gankyrin structures determined by NMR (red) and X-ray crystallography (*54*) (blue).

atoms (residues 4−226) (*54*). Though the N-terminus appears to be well-ordered as described above, the first three residues are missing in the crystal structures (*54*, *55*). Furthermore, C4−S6 residues display relatively large deviations of side chain atoms, which can be partially attributed to the crystal packing force. For example, an NOE was observed between V5 $H^{\gamma 1}$ at 0.26 ppm and W46 $H^{\epsilon 1}$ at 10.96 ppm, whereas the distance between V5 $C^{\gamma 1}$ and W46 $H^{\epsilon 1}$ was measured to be 7.7 Å in the crystal structure (*54*), which is somewhat larger than the NOE limit after correcting for the $C^{\gamma 1}-H^{\gamma 1}$ bond length. Most significant backbone deviations are observed in the C-terminal ankyrin repeat, particularly at G214 and G215, which could be attributed to the paucity of NOE related to these Gly residues (the H^{N} and H^{α} protons of G215 were not assigned).

SUMMARY AND CONCLUSIONS

We have successfully determined the human gankyrin structure under physiological conditions. While the structural studies by NMR and X-ray crystallography complemented each other nicely, the NMR study was clearly a challenge due to the significant homology of the seven ankyrin repeats. Once this difficulty had been overcome, we were able to perform detailed analyses of the structure−function relationship of gankyrin. The NMR studies on H−D exchange provided further insight into the conformational stability of different ankyrin repeats. Detailed NMR analyses of the conserved TPLH motif also led to insight into its structural roles. Building on our previous studies of the structure−function relationship of the INK4 proteins (*27*, *28*, *46*, *57*) and their relationship with gankyrin (*5*), this work has also set a good stage for uncovering the structural basis of the CDK4 binding and Rb binding functions of gankyrin.

SUPPORTING INFORMATION AVAILABLE

2D $^{1}H-^{15}N$ HSQC spectrum with assignments labeled. This material is available free of charge via the Internet at http://pubs.acs.org.

REFERENCES

1. Higashitsuji, H., Itoh, K., Nagao, T., Dawson, S., Nonoguchi, K., Kido, T., Mayer, R. J., Arii, S., and Fujita, J. (2000) Reduced stability of retinoblastoma protein by gankyrin, an oncogenic ankyrin-repeat protein overexpressed in hepatomas, *Nat. Med. 6*, 96−99.
2. Park, T. J., Kim, H. S., Byun, K. H., Jang, J. J., Lee, Y. S., and Lim, I. K. (2001) Sequential changes in hepatocarcinogenesis induced by diethylnitrosamine plus thioacetamide in Fischer 344 rats: induction of gankyrin expression in liver fibrosis, pRB degradation in cirrhosis, and methylation of p16(INK4A) exon 1 in hepatocellular carcinoma, *Mol. Carcinog. 30*, 138−150.
3. Fu, X. Y., Wang, H. Y., Tan, L., Liu, S. Q., Cao, H. F., and Wu, M. C. (2002) Overexpression of p28/gankyrin in human hepatocellular carcinoma and its clinical significance, *World J. Gastroenterol. 8*, 638−643.
4. Dawson, S., Apcher, S., Mee, M., Higashitsuji, H., Baker, R., Uhle, S., Dubiel, W., Fujita, J., and Mayer, R. J. (2002) Gankyrin Is an Ankyrin-repeat Oncoprotein That Interacts with CDK4 Kinase and the S6 ATPase of the 26 S Proteasome, *J. Biol. Chem. 277*, 10893−10902.
5. Li, J., and Tsai, M. D. (2002) Novel insights into the INK4-CDK4/6-Rb pathway: counter action of gankyrin against INK4 proteins regulates the CDK4-mediated phosphorylation of Rb, *Biochemistry 41*, 3977−3983.
6. Nagao, T., Higashitsuji, H., Nonoguchi, K., Sakurai, T., Dawson, S., Mayer, R. J., Itoh, K., and Fujita, J. (2003) MAGE-A4 Interacts with the Liver Oncoprotein Gankyrin and Suppresses Its Tumorigenic Activity, *J. Biol. Chem. 278*, 10668−10674.
7. Sedgwick, S. G., and Smerdon, S. J. (1999) The ankyrin repeat: a diversity of interactions on a common structural framework, *Trends Biochem. Sci. 24*, 311−316.
8. Schultz, J., Milpetz, F., Bork, P., and Ponting, C. P. (1998) SMART, a simple modular architecture research tool: identification of signaling domains, *Proc. Natl. Acad. Sci. U.S.A. 95*, 5857−5864.
9. Li, J., Joo, S. H., and Tsai, M. D. (2003) An NF-κB-specific inhibitor, IκBα, binds to and inhibits cyclin-dependent kinase 4, *Biochemistry 42*, 13476−13483.
10. Salzmann, M., Pervushin, K., Wider, G., Senn, H., and Wuthrich, K. (1998) TROSY in triple-resonance experiments: new perspectives for sequential NMR assignment of large proteins, *Proc. Natl. Acad. Sci. U.S.A. 95*, 13585−13590.
11. Hansen, M. R., Mueller, L., and Pardi, A. (1998) Tunable alignment of macromolecules by filamentous phage yields dipolar coupling interactions, *Nat. Struct. Biol. 5*, 1065−1074.
12. Tjandra, N., and Bax, A. (1997) Direct measurement of distances and angles in biomolecules by NMR in a dilute liquid crystalline medium, *Science 278*, 1111−1114.
13. Cordier, F., Dingley, A. J., and Grzesiek, S. (1999) A doublet-separated sensitivity-enhanced HSQC for the determination of scalar and dipolar one-bond J-couplings, *J. Biomol. NMR 13*, 175−180.
14. Delaglio, F., Grzesiek, S., Vuister, G. W., Zhu, G., Pfeifer, J., and Bax, A. (1995) NMRPipe: a multidimensional spectral processing system based on UNIX pipes, *J. Biomol. NMR 6*, 277−293.
15. Johnson, B. A., and Blevins, R. A. (1994) NMRView: A computer program for the visualization and analysis of NMR data, *J. Biomol. NMR 4*, 603−614.
16. Clore, G. M., Gronenborn, A. M., and Tjandra, N. (1998) Direct structure refinement against residual dipolar couplings in the presence of rhombicity of unknown magnitude, *J. Magn. Reson. 131*, 159−162.
17. Clore, G. M., Gronenborn, A. M., and Bax, A. (1998) A robust method for determining the magnitude of the fully asymmetric alignment tensor of oriented macromolecules in the absence of structural information, *J. Magn. Reson. 133*, 216−226.
18. Dosset, P., Hus, J. C., Marion, D., and Blackledge, M. (2001) A novel interactive tool for rigid-body modeling of multi-domain macromolecules using residual dipolar couplings, *J. Biomol. NMR 20*, 223−231.
19. Clore, G. M., and Garrett, D. S. (1999) R-factor, Free R, and Complete Cross-Validation for Dipolar Coupling Refinement of NMR Structures, *J. Am. Chem. Soc. 121*, 9008−9012.
20. Cornilescu, G., Delaglio, F., and Bax, A. (1999) Protein backbone angle restraints from searching a database for chemical shift and sequence homology, *J. Biomol. NMR 13*, 289−302.
21. Yuan, C., Byeon, I. J., Li, Y., and Tsai, M. D. (1999) Structural analysis of phospholipase A2 from functional perspective. 1. Functionally relevant solution structure and roles of the hydrogen-bonding network, *Biochemistry 38*, 2909−2918.

22. Nilges, M., Clore, G. M., and Gronenborn, A. M. (1988) Determination of three-dimensional structures of proteins from interproton distance data by dynamical simulated annealing from a random array of atoms. Circumventing problems associated with folding, *FEBS Lett. 239*, 129−136.
23. Brunger, A. T., Adams, P. D., Clore, G. M., DeLano, W. L., Gros, P., Grosse-Kunstleve, R. W., Jiang, J. S., Kuszewski, J., Nilges, M., Pannu, N. S., Read, R. J., Rice, L. M., Simonson, T., and Warren, G. L. (1998) Crystallography & NMR system: A new software suite for macromolecular structure determination, *Acta Crystallogr. D54*, 905−921.
24. Laskowski, R. A., Macarthur, M. W., Moss, D. S., and Thornton, J. M. (1993) PROCHECK: a program to check the stereochemical quality of protein structures, *J. Appl. Crystallogr. 26*, 283−291.
25. Koradi, R., Billeter, M., and Wuthrich, K. (1996) MOLMOL: a program for display and analysis of macromolecular structures, *J. Mol. Graphics 14*, 51−55.
26. Luh, F. Y., Archer, S. J., Domaille, P. J., Smith, B. O., Owen, D., Brotherton, D. H., Raine, A. R., Xu, X., Brizuela, L., Brenner, S. L., and Laue, E. D. (1997) Structure of the cyclin-dependent kinase inhibitor p19Ink4d, *Nature 389*, 999−1003.
27. Byeon, I. J., Li, J., Ericson, K., Selby, T. L., Tevelev, A., Kim, H. J., O'Maille, P., and Tsai, M. D. (1998) Tumor suppressor p16INK4A: determination of solution structure and analyses of its interaction with cyclin-dependent kinase 4, *Mol. Cell 1*, 421−431.
28. Li, J., Byeon, I. J., Ericson, K., Poi, M. J., O'Maille, P., Selby, T., and Tsai, M. D. (1999) Tumor suppressor INK4: determination of the solution structure of p18INK4C and demonstration of the functional significance of loops in p18INK4C and p16INK4A, *Biochemistry 38*, 2930−2940.
29. Yuan, C., Selby, T. L., Li, J., Byeon, I. J., and Tsai, M. D. (2000) Tumor suppressor INK4: refinement of p16INK4A structure and determination of p15INK4B structure by comparative modeling and NMR data, *Protein Sci. 9*, 1120−1128.
30. Yang, Y., Nanduri, S., Sen, S., and Qin, J. (1998) The structural basis of ankyrin-like repeat function as revealed by the solution structure of myotrophin, *Structure 6*, 619−626.
31. Gardner, K. H., and Kay, L. E. (1998) The use of ^{2}H, ^{13}C, ^{15}N multidimensional NMR to study the structure and dynamics of proteins, *Annu. Rev. Biophys. Biomol. Struct. 27*, 357−406.
32. Wishart, D. S., and Sykes, B. D. (1994) The ^{13}C chemical-shift index: a simple method for the identification of protein secondary structure using ^{13}C chemical-shift data, *J. Biomol. NMR 4*, 171−180.
33. Pelton, J. G., Torchia, D. A., Meadow, N. D., and Roseman, S. (1993) Tautomeric states of the active-site histidines of phosphorylated and unphosphorylated IIIGlc, a signal-transducing protein from *Escherichia coli*, using two-dimensional heteronuclear NMR techniques, *Protein Sci. 2*, 543−558.
34. Otting, G., and Wuthrich, K. (1989) Extended heteronuclear editing of 2D ^{1}H NMR spectra of isotope-labeled proteins, using the X(ω1,ω2) double half filter, *J. Magn. Reson. 85*, 586−594.
35. Breeze, A. L. (2000) Isotope-filtered NMR methods for the study of biomolecular structure and interactions, *Prog. Nucl. Magn. Reson. Spectrosc. 36*, 323−372.
36. Serrano, L., Sancho, J., Hirshberg, M., and Fersht, A. R. (1992) α-Helix stability in proteins. I. Empirical correlations concerning substitution of side-chains at the N and C-caps and the replacement of alanine by glycine or serine at solvent-exposed surfaces, *J. Mol. Biol. 227*, 544−559.
37. Presta, L. G., and Rose, G. D. (1988) Helix signals in proteins, *Science 240*, 1632−1641.
38. Kohl, A., Binz, H. K., Forrer, P., Stumpp, M. T., Pluckthun, A., and Grutter, M. G. (2003) Designed to be stable: crystal structure of a consensus ankyrin repeat protein, *Proc. Natl. Acad. Sci. U.S.A. 100*, 1700−1705.
39. Binz, H. K., Stumpp, M. T., Forrer, P., Amstutz, P., and Pluckthun, A. (2003) Designing repeat proteins: well-expressed, soluble and stable proteins from combinatorial libraries of consensus ankyrin repeat proteins, *J. Mol. Biol. 332*, 489−503.
40. Bax, A. (2003) Weak alignment offers new NMR opportunities to study protein structure and dynamics, *Protein Sci. 12*, 1−16.
41. Michaely, P., Tomchick, D. R., Machius, M., and Anderson, R. G. (2002) Crystal structure of a 12 ANK repeat stack from human ankyrinR, *EMBO J. 21*, 6387−6396.
42. Leonchiks, A., Liepinsh, E., Barishev, M., Sharipo, A., Masucci, M. G., and Otting, G. (1998) Random coil conformation of a Gly/Ala-rich insert in IκBα excludes structural stabilization as the mechanism for protection against proteasomal degradation, *FEBS Lett. 440*, 365−369.
43. Russo, A. A., Tong, L., Lee, J. O., Jeffrey, P. D., and Pavletich, N. P. (1998) Structural basis for inhibition of the cyclin-dependent kinase Cdk6 by the tumour suppressor p16INK4a, *Nature 395*, 237−243.
44. Crane, E. J., III, Vervoort, J., and Claiborne, A. (1997) ^{13}C NMR analysis of the cysteine-sulfenic acid redox center of enterococcal NADH peroxidase, *Biochemistry 36*, 8611−8618.
45. Dunaief, J. L., King, A., Esumi, N., Eagen, M., Dentchev, T., Sung, C. H., Chen, S., and Zack, D. J. (2002) Protein Phosphatase 1 binds strongly to the retinoblastoma protein but not to p107 or p130 in vitro and in vivo, *Curr. Eye Res. 24*, 392−396.
46. Tevelev, A., Byeon, I. J., Selby, T., Ericson, K., Kim, H. J., Kraynov, V., and Tsai, M. D. (1996) Tumor suppressor p16INK4A: structural characterization of wild-type and mutant proteins by NMR and circular dichroism, *Biochemistry 35*, 9475−9487.
47. Yuan, C., Li, J., Selby, T. L., Byeon, I. J., and Tsai, M. D. (1999) Tumor suppressor INK4: comparisons of conformational properties between p16(INK4A) and p18(INK4C), *J. Mol. Biol. 294*, 201−211.
48. Tang, K. S., Fersht, A. R., and Itzhaki, L. S. (2003) Sequential unfolding of ankyrin repeats in tumor suppressor p16, *Structure 11*, 67−73.
49. Jacobs, M. D., and Harrison, S. C. (1998) Structure of an IκBα/NF-κB complex, *Cell 95*, 749−758.
50. Burley, S. K., and Petsko, G. A. (1986) Amino-aromatic interactions in proteins, *FEBS Lett. 203*, 139−143.
51. Mosavi, L. K., and Peng, Z. Y. (2003) Structure-based substitutions for increased solubility of a designed protein, *Protein Eng. 16*, 739−745.
52. Main, E. R., Jackson, S. E., and Regan, L. (2003) The folding and design of repeat proteins: reaching a consensus, *Curr. Opin. Struct. Biol. 13*, 482−489.
53. Mosavi, L. K., Minor, D. L., Jr., and Peng, Z. Y. (2002) Consensus-derived structural determinants of the ankyrin repeat motif, *Proc. Natl. Acad. Sci. U.S.A. 99*, 16029−16034.
54. Krzywda, S., Brzozowski, A. M., Higashitsuji, H., Fujita, J., Welchman, R., Dawson, S., Mayer, R. J., and Wilkinson, A. J. (2004) The crystal structure of gankyrin, an oncoprotein found in complexes with cyclin-dependent kinase 4, a 19 S proteasomal ATPase regulator, and the tumor suppressors Rb and p53, *J. Biol. Chem. 279*, 1541−1545.
55. Manjasetty, B. A., Quedenau, C., Sievert, V., Bussow, K., Niesen, F., Delbruck, H., and Heinemann, U. (2004) X-ray structure of human gankyrin, the product of a gene linked to hepatocellular carcinoma, *Proteins 55*, 214−217.
56. Padmanabhan, B., Adachi, N., Kataoka, K., and Horikoshi, M. (2004) Crystal structure of the homolog of the oncoprotein gankyrin, an interactor of Rb and CDK4/6, *J. Biol. Chem. 279*, 1546−1552.
57. Li, J., Poi, M. J., Qin, D., Selby, T. L., Byeon, I. J., and Tsai, M. D. (2000) Tumor suppressor INK4: quantitative structure−function analyses of p18INK4C as an inhibitor of cyclin-dependent kinase 4, *Biochemistry 39*, 649−657.

BI049116O